Bending Response of a Book with Internal Friction

Samuel Poincloux [ORCID],[1] Tian Chen [ORCID],[1] Basile Audoly [ORCID],[2,*] and Pedro M. Reis [ORCID][1,†]

[1]*Flexible Structures Laboratory, École Polytechnique Fédérale de Lausanne (EPFL), Lausanne 1015, Switzerland*
[2]*Laboratoire de Mécanique des Solides, CNRS, Institut Polytechnique de Paris, Palaiseau 91128, France*

We study the bending of a booklike system, comprising a stack of elastic plates coupled through friction. The behavior of this layered system is rich and nontrivial, with a nonadditive enhancement of the apparent stiffness and a significant hysteretic response. A dimension reduction procedure is employed to develop a centerline-based theory describing the stack as a nonlinear planar rod with internal shear. We consider the coupling between the nonlinear geometry and the elasticity of the stacked plates, treating the interlayer friction perturbatively. This model yields predictions for the stack's mechanical response in three-point bending that are in excellent agreement with our experiments. Remarkably, we find that the energy dissipated during deformation can be rationalized over 3 orders of magnitude, including the regimes of a thick stack with large deflection. This robust dissipative mechanism could be harnessed to design new classes of low-cost and efficient damping devices.

Multilayered microstructure layouts are essential in many biological and engineered materials for enhanced mechanical properties [1]. For example, nacre and nacre-like materials have been investigated and engineered for their superior stiffness, strength, and toughness [2–4]. Layered architectures are also found across scales, from multilayer graphene [5] and fish scales [6,7] to deployable mechanisms [8] and geological stacks [9]. In all these systems, interlayer interactions dictate the overall mechanical response. Frictional damping across layered elements is also central to the performance of classic engineering systems, such as mechanical joints [10], turbine blades [11], and leaf springs [12,13]. There has been progress in modeling layered system with a few number of interfaces [14–16] or when frictional effects dominate [17]. Still, it remains challenging to predict how the microscopic architecture and interlayer interactions of a layered mechanical system give rise to a specific macroscopic constitutive response, especially for large deformations.

Here, we study the mechanics of a model layered system, where the effects of the small-scale structural layout and friction can be related directly to the macroscopic response. Specifically, we address the question: What is the bending response of a book with internal friction? It is well known that the bending stiffness of a slender structure scales as its thickness cubed $\sim h^3$ [18]. Naturally, the answer for a book with n sheets is bound by the two limiting cases of $\sim (nh)^3$ and $\sim nh^3$. The first estimate ignores the possibility of sliding (infinite friction), whereas the second neglects the interlayer shear stresses (zero friction). As in other related problems studied recently involving friction [17,19,20], there is no general solution method to tackle friction, especially when it couples with other ingredients, such as elasticity, nonlinear

geometry, and multiplicity of contacts. We study this problem by performing precision nonlinear bending tests of a multilayered stack of elastic plates interacting solely through friction [see Fig. 1(a)]. We quantify the mechanical response of this booklike system, including the dissipated
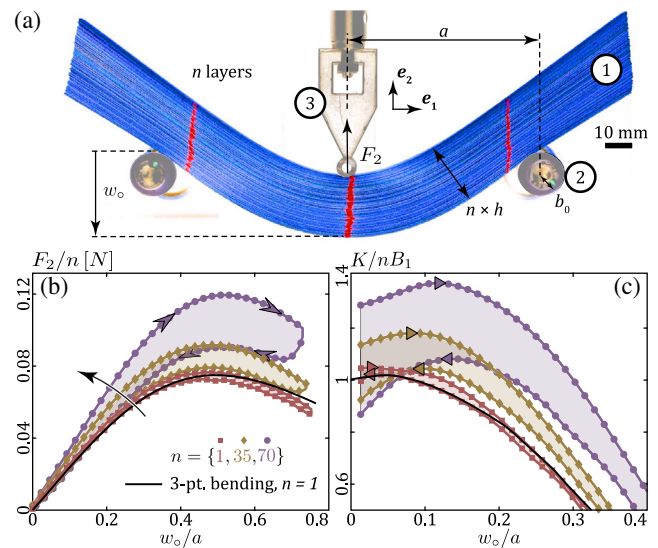

FIG. 1. (a) Photograph (front view) of the experimental setup. A stack ① of n plates ($n = 70$ here) is placed on two rollers ② and loaded by an indenter ③ prescribing the deflection at midspan. (b) Loading-unloading curves of the average indenter force per plate $F_2(w_\circ)/n$ for selected values of n. The thin black line corresponds to the classic, nonlinear prediction for the three-point bending of a single plate, $n = 1$ ([21], Sec. II). (c) Normalized incremental rigidity $K/(nB_1)$ and its maxima $K_m^\pm$ (▷ and ◁ symbols for loading and unloading, respectively).

energy. Following a dimension reduction procedure, we develop a beamlike theory based on the centerline of the stack. This model takes into account the nonlinear geometry of large stacks and treats friction as a perturbation.

In our experiments, we quantify the resistance to bending of a booklike system by performing mechanical tests of a stack of n plates in a three-point bending configuration [see photographs of the apparatus in Fig. 1(a) and the Supplemental Material [21], Sec. I]. This canonical testing geometry is well established for the characterization of the mechanics of beams, including in the large deflection regime [22,23]. We seek to quantify the effect of frictional dissipation between the plates on the mechanical response of the system. Our stack comprises n plates made of polyethylene terephthalate (Partwell group), each with dimensions $2L \times W \times h = 220 \times 30 \times 0.286$ mm^3. The number of plates is varied in the range $1 \leq n \leq 70$. Both faces of the plates are roughened using sandpaper (K80, Emil-Lux GmbH) to avoid interlayer adhesion and ensure reproducible dry-friction interactions [24]. The three-point bending configuration is established by two fixed lower supports, separated by $2a = 130$ mm, and an indenter located at midspan. The fixed supports are set as rollers, comprising two steel cylinders (radius $b_0 = 6.8$ mm) coated with a film of vinyl polysiloxane (thickness ≈ 100 μm) to prevent sliding, and mounted on air bearings (IBS Precision Engineering, pressure ≈ 70 psi) to offer nearly frictionless rotation of the supports. The reaction force at the indenter F_2 is measured by a universal testing machine (Instron 5943) under imposed-displacement conditions. The midspan deflection is cycled at constant speed ($v = \pm 1$ mm/s) in the range $0 \leq w_\circ \leq w_\circ^{\mathrm{max}}$. The geometry and loading conditions ensure that each plate remains in the elastic regime. Our experimental apparatus yields highly reproducible and precise mechanical response measurements (further evidence provided in the Supplemental Material [21], Sec. I).

In Fig. 1(b), we plot representative curves of the average load per plate F_2/n for cycles with amplitude $w_\circ^{\mathrm{max}} = 50$ mm, at selected values of $n = \{1, 35, 70\}$. For $n = 1$, the response agrees with the classic prediction for large-deflection three-point bending; there is a linear regime followed by a maximal load with no hysteresis during unloading (see [21], Sec. II). We find that both the maximal load per layer F_2/n and the energy dissipation through friction (area of the hysteresis loop) increase with n, implying that the behavior of the stack is not a superposition of n independent layers. To address this nonlinear response, we introduce the incremental stiffness $K(w_\circ) = (a^3/6)(dF_2/dw_\circ)$; the prefactor ensures that $K = nB_1$ for small deflection and without friction, where $B_1 = [Eh^3W/12(1 - \nu^2)] = 1.76 \times 10^{-4}$ N m^2 is the bending rigidity of a single plate, $E = 2.4$ GPa is the Young modulus, and $\nu = 0.44$ is Poisson's ratio. In Fig. 1(c), we plot $K(w_\circ)/(nB_1)$, using the same data as in Fig. 1(b), for a loading-unloading cycle. The limiting value

$K(0)/(nB_1)$ for small deflections is 1 for $n = 1$ and increases with n, implying that, when $n > 1$, friction affects even the initial response. In addition, the loading curves display an increasingly pronounced hysteresis as n increases: the incremental stiffness K is different between loading and unloading. The maximum stiffness $K_m^{\pm}$ provides a robust measure of the bending rigidity of the stack; we define one for loading, K_m^+, and one for unloading, K_m^-.

Having characterized the overall loading response of our stacks, we proceed by further quantifying the kinematics of a bent stack. By way of example, we select a thick stack with $n = 70$ and focus on two representative configurations at moderate and large deflections, $w_\circ/a = 0.4$ and 1, see Figs. 2(a1) and 2(a2). The schematic diagram in Fig. 2(c) defines the quantities used in the geometric analysis: θ is the tangent orientation, and $\tilde{S}$ is the arc length measured along a specific plate. In Fig. 2(b), we plot the profiles $\theta(\tilde{S})$ for the upper- and lowermost plates, for the two selected deflection levels. The profiles of the upper- and lowermost plates are different, especially at larger deflections: the same increment of θ takes place over a narrower range of arc length $\tilde{S}$ in the uppermost plate than in the lowermost one. An appropriate model for the stack must account for these through-thickness variations.

We visualize the extent of shear in our booklike system by physically painting three red lines on the lateral face of the stack [see Figs. 2(a)1 and 2(a2)], perpendicularly to its centerline in the undeformed configuration. During the ensuing deformation by the three-point bending test, we find that the two outer lines lose perpendicularity to the centerline, indicating that there is significant shear. The nonpenetration of the contacting plates is at the source of this shear buildup, which is known to arise in parallel bundles of inextensible curves [25]; strong geometric
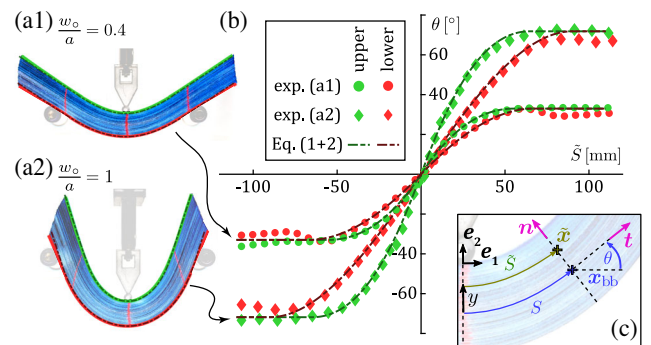

FIG. 2. (a) Snapshots of a deformed stack with $n = 70$, at (a1) $w_\circ/a = 0.4$ (filled disks) and (a2) $w_\circ/a = 1$ (filled diamonds). (b) Schematic diagram of the geometric quantities used in Eq. (1). (c) Tangent angle θ versus arc length $\tilde{S}$ along the upper- and lowermost plates (green and red symbols, respectively). The predictions (dashed lines) were obtained by integrating Eq. (2). The predicted profiles are superimposed as dashed curves in (a1) and (a2).

constraints couple the layers in the stack. A well-known model for thick and shearable beams is that of Timoshenko [26,27]; however, it is inapplicable here as it assumes that the shear stress has an elastic origin.

To rationalize our experimental results, we build a 1D model for thick beams that accounts for internal friction at the interfaces of the layers. Similar reduction methods for bundles of slender components have recently been employed to describe helical strips [28,29] or bundled filaments [30], albeit in different geometries than ours and without considering friction. The centerline of the stack is represented as an inextensible curve $\mathbf{x}_{bb}(S)$ with arc length S and curvature $\kappa(S)$; we reserve the symbol S for arc lengths measured along the stack's centerline, whereas $\tilde{S}$ pertains to the arc length along a specific plate. The transverse coordinate y varies from $-nh/2$ at the lowermost plate to $nh/2$ at the uppermost one. In the absence of delamination, the final position of a point belonging to the plate offset by y from the stack's centerline is written as

$$\tilde{\mathbf{x}}(S, y) = \mathbf{x}_{bb}(S) + \mathbf{n}(S)y, \qquad (1)$$

where $\mathbf{n}(S)$ is the unit normal to the centerline [Fig. 2(c)]. Note that in our non-Lagrangian parametrization, the final position $\tilde{\mathbf{x}}$ is viewed as a function of the arc length S of its *projection* $\mathbf{x}_{bb}$ onto the centerline in the *final* configuration. Thus, S is different from the Lagrangian arc length $\tilde{S}$, and $\tilde{S}(S, y) - S$ provides a measure of shear. The two arc lengths are related as $d\tilde{S} = [1 - y\kappa(S)]dS$ due to the combined effects of curvature and plate inextensibility, as shown in the Supplemental Material ([21], Sec. II) by differentiating Eq. (1).

From Eq. (1), the curvature of a plate is $\tilde{\kappa}(\tilde{S}, y) = \kappa(S)[1 - y\kappa(S)]^{-1}$. The bending energy $\mathcal{E}$ of the stack is found by summing the contributions $\int_{-L}^{+L}(B_1/2)\tilde{\kappa}^2 d\tilde{S}$ from each plate, yielding

$$\mathcal{E} = 2\frac{B_1}{nh^2}\int_0^\ell \varphi[nh\kappa(S)]dS,$$

where $\varphi(x) = (x/2)\ln(1 + \frac{x}{2}/1 - \frac{x}{2})$ and ℓ is the arc length where contact with the rollers takes place, $\ell(w_\circ = 0) = a$ (see [21], Sec. II). The range of the integration to obtain $\mathcal{E}$ has been restricted to $0 \le S \le \ell$, given both the symmetry of the solution and the fact that the overhanging parts of the stack beyond the supports remain straight and, therefore, carry no energy.

The strain energy potential $\mathcal{E}$ defines an equivalent non-linear beam model for the stack, with an internal moment given by the constitutive law $M(S) = (B_1/h)\varphi'(nh\kappa)$. Following a variational approach (see [21], Sec. II), one obtains the governing equilibrium (Kirchhoff) equations for planar rods,

$$\frac{nB_1\theta''(S)}{(1 - \frac{n^2h^2\theta'^2(S)}{2})^2} + \left(\frac{F_2}{2}\cos\theta(S) + F_1\sin\theta(S)\right) = 0, \quad (2)$$

where primes denote differentiation with respect to S, F_2 is the poking force, and the reaction force at the support $S = \pm\ell$ is written as $\mathbf{F} = \mp F_1\mathbf{e_1} + (F_2/2)\mathbf{e_2}$. The centerline satisfies $x_1'(S) = \cos\theta(S)$ and $x_2'(S) = \sin\theta(S)$. The boundary conditions are $(\theta, x_1, x_2)_{S=0} = (0, 0, -w_\circ)$ and $(\theta', x_1, x_2)_{S=\ell} = (0, a - b\sin\theta(\ell), b(\cos\theta(\ell) - 1))$, with $b = b_0 + nh/2$ as the effective radius of the support.

Solving the boundary-value problem in Eq. (2) yields the centerline $\mathbf{x}_{bb}(S)$; this solution ignores friction and will be referred to as the "elastic backbone." The shape of the full stack can be reconstructed using Eq. (1). In Fig. 2(a), we find excellent agreement between the computed and the experimental shapes of the upper- and lowermost plates. As part of the solution process, one also obtains the poking force $F_{2,bb}(w_\circ)$.

Next, we address the interlayer friction to rationalize the hysteresis observed in the experiments. Treating friction as a perturbation, we use the (frictionless) elastic backbone solution obtained above to estimate the power $\mathcal{P}_\mu$ dissipated by friction. This $\mathcal{P}_\mu$ is the integral over all the plate-plate interfaces of the sliding velocity multiplied by the tangential contact stress. From Amontons-Coulomb law of friction, the tangential contact stress is the friction coefficient μ times the normal stress $\Sigma(S, y)$. Given that the plates are sliding against one another, μ is a dynamic friction coefficient. Reconstructing the stress $\Sigma(S, y)$ in the backbone solution and carrying out a partial integration in the transverse direction, one obtains the expression of the dissipated power as ([21], Sec. III)

$$\mathcal{P}_\mu = \mu hn|\mathbf{F}||\dot{\theta}(\ell)| + 2\mu\int_0^\ell Q(S)|\dot{\theta}(S)|dS, \quad (3)$$

where dots denotes differentiation with respect to time and $Q(S) = \int_{-nh/2}^{nh/2}|\Sigma(S, y)|dy$.

The first term in Eq. (3) represents the dissipation in the stack by the pointlike contact force at the supports, while the second term is the dissipation everywhere else in the stack. By symmetry, there is no sliding (hence, no dissipation) at the poking point. The poking force is then derived by a global balance of power as

$$F_2\dot{w}_\circ = -\dot{\mathcal{E}} + \mathcal{P}_\mu. \quad (4)$$

Whereas $\dot{w}_\circ$ and $\dot{\mathcal{E}}$ change sign between loading and unloading, $\mathcal{P}_\mu$ does not, implying that F_2 is different during the two phases.

Before the poking force can be computed from Eqs. (3) and (4), the kinematic friction coefficient μ must be obtained. Friction coefficients for dry surfaces are known to be sensitive to the magnitude of the normal load [17],
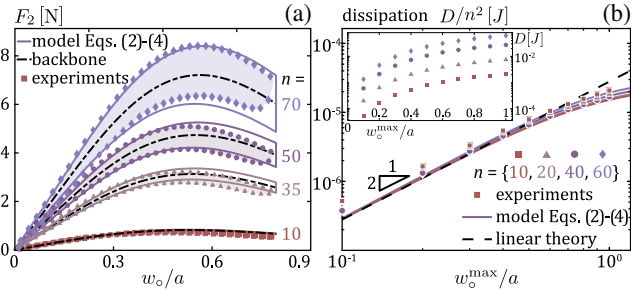
FIG. 3. Predictions of the model from Eqs. (2)–(4), solid lines, superposed onto the experimental data (points), for stacks with different numbers of layers. (a) Load-deflection response, for loading and unloading cycles. $n = \{10, 35, 50, 70\}$. Dash-dotted line corresponds to the elastic backbone (without friction). (b) Scaled energy dissipated in the stack D/n^2 per cycle, as a function of the scaled deflection $w_\circ^{\max}/a$. Inset: raw data for D versus $w_\circ^{\max}/a$. $n = \{10, 20, 40, 60\}$.

which, in our system, varies significantly depending on both the amount of deflection and the position along the stack ([21], Sec. III). Therefore, an independent measurement of μ may not be relevant. Instead, we proceed by extracting μ directly from the experimental data by leveraging the variations of the stacks stiffness $K_m^{\pm}$ as a function of n. In the limit of small deflections (see Supplemental Material [21], Sec. IV), our model yields $K_m^{\pm} = K_{m\mathrm{bb}} \times [1 \pm n\mu\frac{3}{4}(h/a)]$ with $K_{m\mathrm{bb}}$ as the bending stiffness of the backbone solution; with the scaling $K_{m\mathrm{bb}} \sim nEh^3W$, this yields $K_m^{\pm} \sim nEh^3W[1 \pm n\mu\frac{3}{4}(h/a)]$, which is in-line with the nh^3 scaling anticipated in the Introduction while also including the correction from friction. Exploiting the linear relation between $K_m^{\pm}/K_{m\mathrm{bb}}$ and n provides the friction coefficient as $\mu = 0.52 \pm 0.03$ (see [21], Sec. V for more details on how $K_m^{\pm}$ and μ were obtained from the experimental data). The poking force F_2 can now be obtained from Eqs. (2)–(4) to compute the loading curves over the entire deflection range. In Fig. 3(a), we compare the predictions from our model (solid curves) with the experiments (data points), finding excellent agreement between the two, for different values of n, with a single parameter μ that was fitted to the data once and for all.

In Fig. 3(b), the energy D dissipated during one loading cycle is plotted as a function of the scaled maximum deflection. From the experimental data, D is measured as the area enclosed by the loading-unloading curves. The model predictions are accurate over the entire range of parameters, from thin to thick stacks and small to large deflections; i.e., $10 \leq n \leq 60$ and $0.1 \leq w_\circ^{\max}/a \leq 1$, respectively. For small deflections, the curves collapse onto a straight line in the logarithmic plot, corresponding to the power law $D_{\mathrm{lin}} = (9\mu B_1 h/2a^2)(nw_\circ^{\max}/a)^2$ applicable to small deflections (see [21], Sec. IV).

In closing, we highlight that the ability of our centerline-based theory to accurately capture the mechanical behavior

of a stack of frictional plates was *a priori* not straightforward, given the nonconservative nature of the system. We circumnavigated this challenge by treating friction perturbatively while tracking the localized dissipative regions and considering the full coupling between elasticity and nonlinear geometry. Our methodology is general and we anticipate that it can be adapted to other complex systems where friction is important. We have uncovered a simple mechanism where the energy dissipated per cycle can be made to vary by a large amount; this could be harnessed to design new classes of low-cost and efficient damping devices. As geometry, elasticity, and friction are the sole ingredients, it should be applicable across a wide range of length scales. Whereas we focused on a quasistatic setting, dynamic and impact conditions should also be included in future research efforts, which we hope the current study will instigate.

[*]basile.audoly@polytechnique.edu
[†]pedro.reis@epfl.ch

[1] J. R. Vinson, Appl. Mech. Rev. **54**, 201 (2001).
[2] A. Jackson, J. F. Vincent, and R. Turner, Proc. R. Soc. B **234**, 415 (1988).
[3] Z. Tang, N. A. Kotov, S. Magonov, and B. Ozturk, Nat. Mater. **2**, 413 (2003).
[4] Z. Yin, F. Hannard, and F. Barthelat, Science **364**, 1260 (2019).
[5] G. Wang, Z. Dai, J. Xiao, S. Z. Feng, C. Weng, L. Liu, Z. Xu, R. Huang, and Z. Zhang, Phys. Rev. Lett. **123**, 116101 (2019).
[6] B. J. Bruet, J. Song, M. C. Boyce, and C. Ortiz, Nat. Mater. **7**, 748 (2008).
[7] H. Ali, H. Ebrahimi, and R. Ghosh, Sci. Rep. **9**, 14628 (2019).
[8] J. A. Umali, L. L. Wilson, and S. Pellegrino, *4th AIAA Spacecraft Structures Conference* (American Institute of Aeronautics and Astronautics, 2017), p. 1115, https://doi.org/10.2514/6.2017-1115.
[9] J. Q. Ran, E. K. S. Passaris, and P. Mottahed, Rock mechanics and rock engineering **27**, 235 (1994).
[10] S. Bograd, P. Reuss, A. Schmidt, L. Gaul, and M. Mayer, Mech. Syst. Signal Process. **25**, 2801 (2011).
[11] J. H. Griffin, Int. J. Turbo Jet Engines **7**, 297 (1990).
[12] F. Badrakhan, J. Sound Vib. **174**, 91 (1994).
[13] M. Osipenko, Y. Nyashin, and R. Rudakov, Int. J. Solids Struct. **40**, 3129 (2003).
[14] S. Hansen and R. Spies, J. Sound Vib. **204**, 183 (1997).
[15] H. M. Sedighi, K. H. Shirazi, and K. Naderan-Tahan, J. Acoust. Vib. **135**, 061006 (2013).
[16] H. K. Asker, J. A. Rongong, and C. E. Lord, Mech. Syst. Signal Process **101**, 168 (2018).
[17] H. Alarcón, T. Salez, C. Poulard, J.-F. Bloch, E. Raphaël, K. Dalnoki-Veress, and F. Restagno, Phys. Rev. Lett. **116**, 015502 (2016).

[18] B. Audoly and Y. Pomeau, *Elasticity and Geometry* (Oxford University Press, New York, 2010).

[19] M. K. Jawed, P. Dieleman, B. Audoly, and P. M. Reis, Phys. Rev. Lett. **115**, 118302 (2015).

[20] H. Shlomai, D. S. Kammer, M. Adda-Bedia, and J. Fineberg, Proc. Natl. Acad. Sci. U.S.A. **117**, 13379 (2020).

[21] See Supplemental Material at http://link.aps.org/supplemental/10.1103/PhysRevLett.126.218004 for additional evidence on the experimental reproducibility, details on the derivations of the model, and measurement of the effective friction coefficient.

[22] A. Ohtsuki, Bull. Jpn. Soc. Mech. Eng. **29**, 1988 (1986).

[23] M. Batista, Int. J. Nonlinear Mech. **69**, 84 (2015).

[24] T. Baumberger and C. Caroli, Adv. Phys. **55**, 279 (2006).

[25] B. Pham, Computer Aided Design **24**, 223 (1992).

[26] S. P. Timoshenko, London Edinburgh Philos. Mag. J. Sci. **41**, 744 (1921).

[27] D.-K. Li and X.-F. Li, C. R. Méc. **344**, 556 (2016).

[28] H. S. Ansell, D. S. Kim, R. D. Kamien, E. Katifori, and T. Lopez-Leon, Phys. Rev. Lett. **123**, 157801 (2019).

[29] G. Noselli, M. Arroyo, and A. DeSimone, J. Mech. Phys. Solids **123**, 234 (2019).

[30] D. W. Atkinson, C. D. Santangelo, and G. M. Grason, New J. Phys. **21**, 062001 (2019).